



OPEN ACCESS

EDITED BY

Hong Zhao,
Auburn University, United States

REVIEWED BY

Binbin Ni,
Wuhan University, China
Huayue Chen,
Auburn University, United States

*CORRESPONDENCE

Poorya Hosseini,
✉ poorya.hosseini@ucdenver.edu

RECEIVED 21 August 2024

ACCEPTED 23 October 2024

PUBLISHED 06 November 2024

CITATION

Hosseini P, Harid V, Gotkowski M and Tu W (2024) Backward test particle simulation of nonlinear cyclotron wave-particle interactions in the radiation belts. *Front. Astron. Space Sci.* 11:1484399. doi: 10.3389/fspas.2024.1484399

COPYRIGHT

© 2024 Hosseini, Harid, Gotkowski and Tu. This is an open-access article distributed under the terms of the [Creative Commons Attribution License \(CC BY\)](https://creativecommons.org/licenses/by/4.0/). The use, distribution or reproduction in other forums is permitted, provided the original author(s) and the copyright owner(s) are credited and that the original publication in this journal is cited, in accordance with accepted academic practice. No use, distribution or reproduction is permitted which does not comply with these terms.

Backward test particle simulation of nonlinear cyclotron wave-particle interactions in the radiation belts

Poorya Hosseini^{1,2*}, Vijay Harid¹, Mark Gotkowski¹ and Weichao Tu²

¹Department of Electrical Engineering, University of Colorado Denver, Denver, CO, United States,

²Department of Physics and Astronomy, West Virginia University, Morgantown, WV, United States

Wave-particle interaction plays a crucial role in the dynamics of the Earth's radiation belts. Cyclotron resonance between coherent whistler mode electromagnetic waves and energetic electrons of the radiation belts is often called a coherent instability. Coherent instability leads to wave amplification/generation and particle acceleration/scattering. The effect of wave on particle's distribution function is a key component of the instability. In general, whistler wave amplitude can grow over threshold of quasi-linear (linear) diffusion theory which analytically tracks the time-evolution of a particle distribution. Thus, a numerical approach is required to model the nonlinear wave induced perturbations on particle distribution function. A backward test particle model is used to determine the energetic electrons phase space dynamics as a result of coherent whistler wave instability. The results show the formation of a phase space features with much higher resolution than is available with forward scattering models. In the nonlinear regime the formation of electron phase space holes upstream of a monochromatic wave is observed. The results validate the nonlinear phase trapping mechanism that drives nonlinear whistler mode growth. The key differences in phase-space perturbations between the linear and nonlinear scenarios are also illustrated. For the linearized equations or for low (below threshold) wave amplitudes in the nonlinear case, there is no formation of a phase-space hole and both models show features that can be characterized as linear striations or ripples in phase-space.

KEYWORDS

gyroresonance, test particle, radiation belt, magnetosphere, plasma wave

1 Introduction

The Earth's magnetosphere can support various electromagnetic wave modes that play a vital role in near-Earth space dynamics. These electromagnetic waves of which the whistler mode is of particular importance, concurrently interact with higher energy radiation belt particles which are trapped in a magnetic mirror configuration of the geomagnetic field (Bell and Buneman, 1964; Helliwell, 1965; Kennel and Petschek, 1966; Lyons et al., 1972; Gendrin, 1981; Omura et al., 1991; Bortnik et al., 2008). Two primary aspects of whistler mode wave-particle interactions are the amplification of the waves by an unstable hot particle distribution, and the precipitation and/or acceleration of these particles by the waves. In general, modeling wave amplification along with particle

scattering and acceleration is a difficult problem that requires a self-consistent solution to the Vlasov-Maxwell system of equations. Several researchers have approached the self-consistent problem using particle-in-cell (PIC) or hybrid simulations (Kato and Omura, 2007; Gibby et al., 2008; Hikishima et al., 2010; Omura and Nunn, 2011; Wang et al., 2024); however, such computationally intensive self-consistent simulations can be unnecessary in scenarios where particle induced modifications to the wave are small and particle scattering by the waves is of greater interest. In other words, to investigate particle dynamics while minimizing computational costs, the test particle method can be employed, where the feedback of particles on the waves is neglected.

A common approach is to specify the wave-fields and neglect feedback from the particles which results in a simpler but only approximate system of equations. For small amplitude and incoherent signals such as plasmaspheric hiss, quasi-linear diffusion theory is a common method to track the time-evolution of a particle distribution (Kennel and Petschek, 1966; Inan et al., 1978; Abel and Thorne, 1998; Albert, 1999; Summers, 2005). For arbitrary wave-fields (which can go beyond the scope of linear theory), however, the dynamics of the particle distribution may need to be investigated using test particle simulations (Maldonado et al., 2016; Fu et al., 2019) or other methods (Hu and Krommes, 1994). Although test particle simulations have been successful in previous work, simulations with large-amplitude and coherent waves can still require many millions of particles to accurately describe the nonlinear phase-space dynamics of the particle distribution function (Dysthe, 1971; Matsumoto and Omura, 1981; Bell, 1984; Gibby et al., 2008; Nunn, 1974; Albert et al., 2012).

In order to alleviate the computational cost of traditional test-particle methods, a more efficient backward test particle solution to the Vlasov equation is employed here to evaluate the nonlinear effects of large-amplitude coherent waves on the energetic particle distribution function. The backward test particle approach exploits the conservation of phase space as articulated in Louisville's theorem and permits determination of the prior state of a particle distribution if the wave-fields are known. Practically, this technique allows regions of interest in phase-space to be defined *a priori* which thus greatly reduces the number of particles that need to be tracked in the simulations and avoids complications from potential under sampling. The method has been previously utilized to efficiently model particle precipitation by coherent whistler mode waves since the loss-cone is well defined (Harid et al., 2014; Nunn and Omura, 2015). In addition, the technique is well-suited for analyzing acceleration to high energies and second-scale variations to the particle distribution function. In this work, the detailed temporal dynamics of the nonlinear wave-induced trap in phase-space are shown at a higher resolution than has been shown in previous works by full PIC (Figure 7 in Hikishima and Omura, 2012) or hybrid (Figure 4.9 in Harid, 2015) simulations. This high resolution allows for the accurate determination of "scattered" fields to investigate salient features of amplified and triggered magnetospheric waves.

2 Theory

The mathematical basis of modeling wave-particle interactions is *via* the Vlasov-Maxwell system of equations. The Vlasov equation

governs the evolution of electron (with mass of m , and charge of q) phase space density $f(\mathbf{r}, \mathbf{v})$ in a collision-free plasma, as:

$$\frac{\partial f}{\partial t} + \mathbf{v} \cdot \frac{\partial f}{\partial \mathbf{r}} - \frac{q}{m} (\mathbf{E}_{\omega} + \mathbf{v} \times \mathbf{B}) \cdot \frac{\partial f}{\partial \mathbf{v}} = 0. \quad (1)$$

where the quantities \mathbf{r} and \mathbf{v} correspond to the position and velocity coordinates of phase-space. \mathbf{E}_{ω} corresponds to the wave electric field while \mathbf{B} is the total magnetic field. The total magnetic field can be decomposed into $\mathbf{B} = \mathbf{B}_{\omega} + \mathbf{B}_0$ where \mathbf{B}_{ω} is the wave magnetic field and \mathbf{B}_0 represents the background geomagnetic field. The Earth's magnetic field retains a dipole shape in the inner magnetosphere, and forces radiation belt electrons to experience helical motion around the background field. The electrons can constantly interact with the circularly polarized whistler mode waves that are propagating along the field line. Here, the waves are assumed to propagate parallel to the magnetic field lines and other (non-whistler mode) wave modes are ignored.

For a circularly polarized whistler mode wave with frequency ω and wavenumber k that is propagating parallel to the background magnetic field lines ($-z$ direction), the expression for the wave magnetic field, \mathbf{B}_{ω} , in Cartesian coordinates is:

$$\mathbf{B}_{\omega} = \Re \left[(\hat{x} - j\hat{y}) B_{\omega} e^{j(\phi_{\omega} + \omega t + \int k dz)} \right] \quad (2)$$

Counter streaming electrons that travel at the appropriate positive velocity will experience an approximately static wave fields and significant energy exchange. This is referred to as Doppler shifted cyclotron resonance or gyro-resonance where resonance velocity (v_r) is given by Equation 3:

$$v_r = \frac{\frac{\omega_c}{\gamma} - \omega}{k} \quad (3)$$

The terms ω_c is the electron cyclotron frequency ($\omega_c = \frac{qB_0}{m}$, where $B_0 = |\mathbf{B}_0|$) and γ is known as the Lorentz factor ($\gamma = \sqrt{1 + \frac{|\mathbf{p}|^2}{m^2 c^2}}$, where $c = \frac{1}{\sqrt{\mu_0 \epsilon_0}}$) which is included to take relativistic corrections into account.

Maxwell's equations govern the evolution of the wave electric and magnetic fields, but the wave equations in a magneto-plasma can be simplified under the assumption of a narrowband modulating wavepacket, given the coherence of the signals observed in the data. The term $\omega t + \int k dz$ in Equation 2 corresponds to the phase variation of a monochromatic plane wave and can be thought of as a feature of an injected (incident) carrier wave. It is worth mentioning, although the focus of the current study is on a monochromatic wave with a singular frequency, waves with a finite but narrow bandwidth are also called narrowband waves and can lead to nonlinear wave-particle interactions. The quantity $B_{\omega} e^{j\phi_{\omega}}$ corresponds to the complex wavepacket that modulates the carrier whistler wave. Both the amplitude (B_{ω}) and phase (ϕ_{ω}) of the modulating wavepacket will be slowly varying functions of position and time, even if the quantity $B_{\omega} e^{j\phi_{\omega}}$ may be varying rapidly. Under the slowly-varying or narrowband assumption the evolution equations for the amplitude and phase of the modulating wavepacket can be simplified as (Nunn, 1974; Matsumoto and Omura, 1981; Omura and Nunn, 2011; Gibby et al., 2008):

$$\left(\frac{\partial}{\partial t} - |v_g| \frac{\partial}{\partial z} \right) B_{\omega} = -\frac{\mu_0 v_g}{2} J_E \quad (4)$$

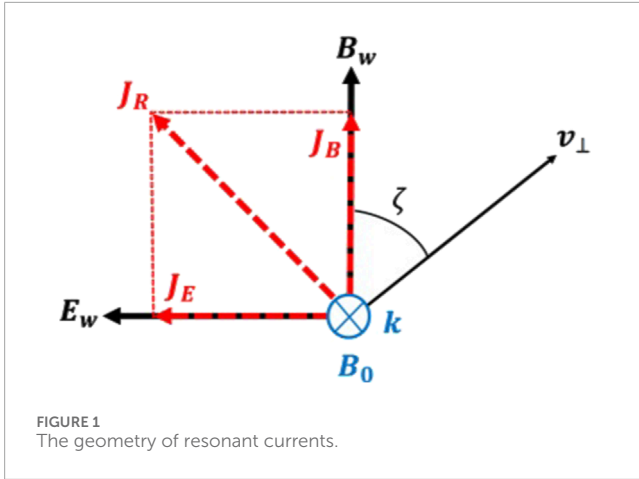


FIGURE 1
The geometry of resonant currents.

$$\left(\frac{\partial}{\partial t} - |v_g| \frac{\partial}{\partial z}\right) \phi_{\omega} = -\frac{\mu_0 v_g}{2} \frac{J_B}{B_{\omega}} \quad (5)$$

These narrowband wave equations have the advantage of separately quantifying the effect of the wave growth and frequency change and can provide useful physical intuition behind the evolution of a wavepacket that is propagating at the group velocity (v_g) of the whistler wave. Specifically, Equation 4 shows that the wave amplitude is driven by the component of the resonant current that is in the direction of the wave electric field (J_E). For a coherent wavepacket, it is assumed that the wave electric field, E_{ω} , is given by, $E_{\omega} = v_p B_{\omega}$, where v_p is the phase-velocity of the wave.

The geometry of the resonant currents (J_R) with respect to the wave fields due to the energetic electrons are delineated in Figure 1. The variables v_{\parallel} (p_{\parallel}) and v_{\perp} (p_{\perp}) are parallel and perpendicular components of electron velocity (momentum) relative to the background geomagnetic field (B_0). The angle between v_{\perp} and B_w ($-B_w$) is referred to as the gyrophase ζ (φ). The quantities J_E and J_B are orthogonal components of resonant currents ($J_R = J_B + \mathcal{J}J_B$) and requires computing the appropriate integral directly over the phase space distribution function (f) in cylindrical (v_{\perp} , v_{\parallel} , φ) coordinate system, which is given by Equations 6, 7, respectively:

$$J_E = q \int f v_{\perp}^2 \sin \varphi dv_{\parallel} dv_{\perp} d\varphi \quad (6)$$

$$J_B = q \int f v_{\perp}^2 \cos \varphi dv_{\parallel} dv_{\perp} d\varphi \quad (7)$$

The dynamics of resonant electrons in a monochromatic whistler mode wave field (B_{ω} , E_{ω}) immersed in a background inhomogeneous magnetic field ($\frac{\partial \omega_c}{\partial z}$), is in general governed by the Lorentz force.

$$\frac{dz}{dt} = v_{\parallel} \quad (8)$$

$$\frac{dp_{\parallel}}{dt} = \frac{q}{m\gamma} B_{\omega} p_{\perp} \sin \zeta - \frac{p_{\perp}^2}{2m\gamma\omega_c} \frac{\partial \omega_c}{\partial z} \quad (9)$$

$$\frac{dp_{\perp}}{dt} = -q \sin \zeta (E_{\omega} + v_{\parallel} B_{\omega}) + \frac{p_{\parallel} p_{\perp}}{2m\gamma\omega_c} \frac{\partial \omega_c}{\partial z} \quad (10)$$

$$\frac{d\zeta}{dt} = k(v_r - v_{\parallel}) - \frac{q \cos \zeta}{p_{\perp}} (E_{\omega} + v_{\parallel} B_{\omega}) \quad (11)$$

where p_{\parallel} (p_{\perp}) are parallel (perpendicular) components of electron momentum relative to the background geomagnetic field. If only electrons that are close to resonance are examined and the small contribution of centripetal acceleration due to the wave is neglected, the equations of motion can be written as Golkowski et al. (2019):

$$\frac{d\zeta}{dt} = \theta \quad (12)$$

$$\frac{d\theta}{dt} = \omega_{tr}^2 (\sin \zeta + \mathcal{S}) \quad (13)$$

Here the variable $\theta = k(v_{\parallel} - v_r)$ represents a normalized change of the electron's parallel velocity from resonance. The quantity $\omega_{tr} = \sqrt{\frac{qk v_{\perp} B_{\omega}}{m}}$ is known as the trapping frequency. The quantity \mathcal{S} is called the "S-parameter" and is a collective inhomogeneity factor based on Equation 14 which quantifies the effect of background inhomogeneity ($\frac{\partial \omega_c}{\partial z}$) as well as the frequency sweep rate observed by the particle ($\frac{d\omega}{dt}$):

$$\mathcal{S} = \frac{1}{\omega_{tr}^2} \left[\left(\frac{kv_{\perp}^2}{2\omega_c} + \frac{3}{2} v_r \right) \frac{\partial \omega_c}{\partial z} + \frac{2\omega + \omega_c}{\omega} \frac{d\omega}{dt} \right] \quad (14)$$

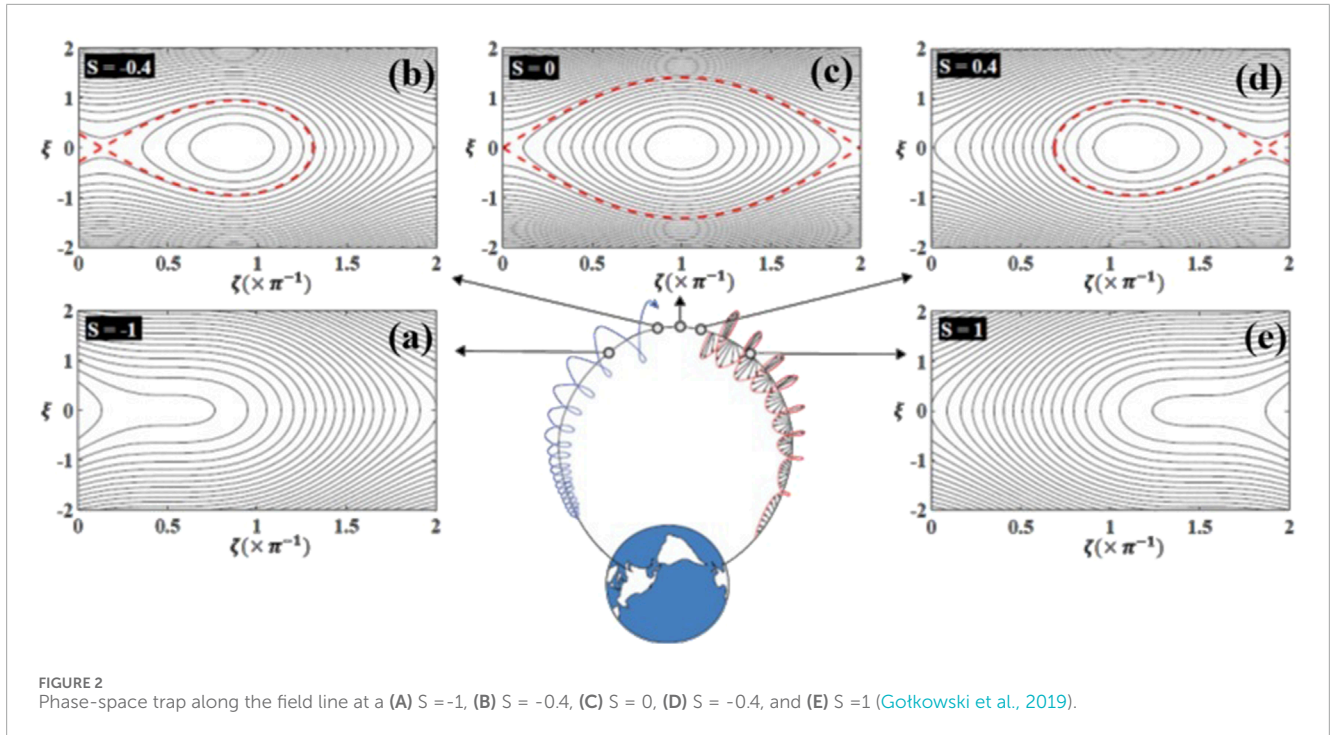
Differentiating Equation 12 with respect to time and plugging into Equation 13, results in a nonlinear ordinary differential equation which represents a forced pendulum equation where the forcing term is proportional to \mathcal{S} :

$$\frac{d^2 \zeta}{dt^2} = \omega_{tr}^2 (\sin \zeta + \mathcal{S}) \quad (15)$$

For $\mathcal{S} = 0$, Equation 15 takes the form of a conventional pendulum equation and the particle will oscillate around $\zeta = \pi$ at the trapping frequency ω_{tr} in a manner similar to which a pendulum oscillates in a constant gravitational field. For values in the range $-1 < \mathcal{S} < 1$, the central phase angle around which the particle oscillates is moved to $\zeta_0 = -\sin^{-1} \mathcal{S}$.

Of particular importance is the formation of a wave-induced trap in phase-space which changes structure depending on the location along the geomagnetic field line. Figure 2 shows the shape of the phase-space trap at several positions (for a monochromatic whistler mode wave) (Golkowski et al., 2019). The variable ξ on the vertical axis is defined by $\frac{\theta}{\sqrt{2}\omega_{tr}}$ and is essentially a normalized deviation of v_{\parallel} from resonance.

The trapped trajectories correspond to closed curves in phase-space while the untrapped particles follow open curves. The trapped and untrapped electron populations are separated by a boundary known as a separatrix and are shown by the red contours. Formally, the separatrix can only exist when $-1 < \mathcal{S} < 1$. If the background magnetic field were homogenous ($\mathcal{S} = 0$), then the initially trapped electrons stay trapped and untrapped particles stay untrapped indefinitely. However, for a spatially dependent \mathcal{S} , this is not necessarily the case. Electrons can either swing around the trap or be trapped for many trapping periods before being detrapped. The exact dynamics are strongly dependent on the initial phase angle, energy, and pitch angle of the electrons. Therefore, by setting $|S| = 1$, the minimum amplitude required for phase trapping, $B_{tr} = \frac{m}{qk v_{\perp}} \left[\frac{kv_{\perp}^2}{2\omega_c} + \frac{3}{2} v_{\parallel} \right] \left| \frac{\partial \omega_c}{\partial z} \right|$, can be obtained.



3 Backward test particle model

The backward test particle numerical model essentially solves the Vlasov Equation 1 for a given wave at a particular location along the geomagnetic field line. Since the Vlasov equation is an advective-type partial differential equation (PDE), information propagates around phase space in a complicated manner. An accurate method of computing the distribution is by using the method of characteristics, which in the context of Vlasov equation is equivalent to Liouville's theorem. By neglecting the transverse spatial motion of electrons and only considering spatial variation along the field line, the Vlasov Equation 1, can be written as Equation 16:

$$\frac{\partial f}{\partial t} + \left(\frac{dz}{dt}\right) \frac{\partial f}{\partial z} + \left(\frac{dp_{\parallel}}{dt}\right) \frac{\partial f}{\partial p_{\parallel}} + \left(\frac{dp_{\perp}}{dt}\right) \frac{\partial f}{\partial p_{\perp}} + \left(\frac{d\varphi}{dt}\right) \frac{\partial f}{\partial \varphi} = 0 \quad (16)$$

where the terms in parenthesis corresponds to equations of motion in Equations 8–11. This is done by considering characteristic curves, which are curves along which the distribution function is advected. This turns the PDE into a set of ODEs. More specifically, consider a general advection equation as:

$$\frac{\partial f}{\partial t} + \vec{c}(\mathbf{r}) \frac{\partial f}{\partial \mathbf{r}} = 0 \quad (17)$$

This type of equation describes advection of the quantity $f(t, \mathbf{r})$ at "speed" \vec{c} at "position" \mathbf{r} . To find the characteristics, we find the trajectories, $\mathbf{r}(t)$ for which the total derivative vanishes as shown in Equation 18:

$$\frac{df(t, \mathbf{r})}{dt} = \frac{\partial f}{\partial t} + \frac{d\mathbf{r}}{dt} \frac{\partial f}{\partial \mathbf{r}} = 0 \quad (18)$$

The original advection Equation 17 can only be satisfied if $\frac{d\mathbf{r}}{dt} = \vec{c}$ is satisfied. Another interpretation is that in the frame of

reference moving at speed \vec{c} , the quantity f does not change. Thus, by solving for the trajectories, we find the curves along which f is advected (Harid et al., 2014). In the case of the Vlasov equation, the characteristic curves are found by solving Equations 8–11. This means the value of the distribution function at any particular point can be determined by tracing the characteristic curves back until time zero. This method requires a grid generated over $(\varphi, v_{\parallel}, \alpha)$ in phase space at any position of interest, z , within the interaction region. The characteristics are traced backward (formally $dt \rightarrow -dt$ for the equations of motion and narrowband wave equations) until time zero.

The simulations use an interaction region that is approximately ± 2000 km around the geomagnetic equator. The phase space grid has $N_{v_{\parallel}} \times N_{\alpha} \times N_{\varphi} = 200 \times 50 \times 32 = 320000$ grid points. All simulations are performed using a centered dipole geomagnetic field model. We use the cold density model from Carpenter and Anderson (1992) to determine the cold plasma parameters under quiet geomagnetic conditions. At $L = 4.9$, the equatorial gyrofrequency is $f_c = 6.8$ kHz; the simulations use an input wave frequency of $f_0 = \frac{f_c}{2} = 3.4$ kHz and a cold plasma density of $N_c = 400 \frac{e1}{cm^3}$. A subtracted bi-Maxwellian distribution of particles is considered for the energetic electrons, which is given by Equation 19:

$$f(p_{\parallel}, p_{\perp}) = C_b e^{-\frac{p_{\parallel}^2}{2p_{th\parallel}^2}} \left[e^{-\frac{p_{\perp}^2}{2p_{th\perp}^2}} - e^{-\frac{p_{\perp}^2}{2\beta p_{th\perp}^2}} \right] \quad (19)$$

where the parameter β determines depletion level of the loss cone distribution, such that $\beta = 0$ refers to a pure bi-Maxwellian and larger values of β give a more depleted loss cone. The quantities p_{\parallel} and p_{\perp} are the particle momenta parallel and perpendicular to the geomagnetic field, respectively. Additionally, $C_b = \frac{N_h}{(1-\beta)p_{th\parallel}p_{th\perp}^2(\sqrt{2\pi})^3}$, where N_h is the hot plasma density, and $p_{th\parallel}$ ($p_{th\perp}$) represents

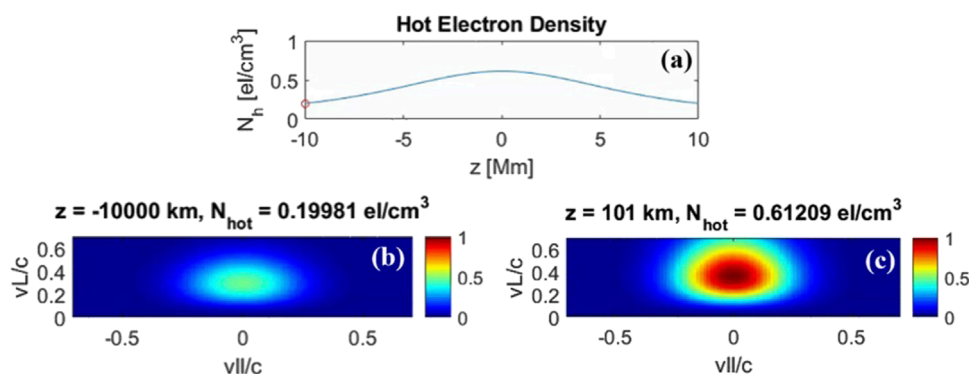


FIGURE 3 (A) Hot electron density as a function of position along the field line, and Subtracted bi-Maxwellian distribution function at a distance (B) $-10,000$ km and (C) 101 km from the magnetic equator, with $\beta = 0.5$. c is the speed of light.

the average hot plasma momenta parallel (perpendicular) to the geomagnetic field. All simulations use $p_{th_{\parallel}} = 0.17c$ and $p_{th_{\perp}} = 0.4c$ where c is the speed of light in free space. Such a distribution represents a Maxwellian distribution without the loss cone particles that would be absent in the magnetosphere. Figure 3A shows the hot electron density as a function of position along the field line. Figures 3B, C shows a color-map of the phase-space subtracted bi-Maxwellian distribution function at a distance $-10,000$ km and 101 km from the magnetic equator, respectively. As shown, the distribution function is higher at high pitch angles which is characteristic of the radiation belt population. The rapid decay of particle density (away from $z = 0$) due to the magnetic bottle configuration is clearly demonstrated in Figure 3A and is consistent with the interaction region being dominated by the near-equatorial region.

The wave fields are taken into account by illuminating the entrance of the interaction region with an input signal and using this as a boundary condition for the wave equations. A fourth-order Runge-Kutta (RK4) time-stepping scheme is used to evolve Equations 8–11. The wave equation is time stepped using a semi-Lagrangian scheme with cubic spline interpolation.

For a distribution function of this form, the pitch angle anisotropy is given by $A = \beta \frac{p_{th_{\perp}}^2}{p_{th_{\parallel}}^2} + \left(\frac{p_{th_{\perp}}^2}{p_{th_{\parallel}}^2} - 1 \right)$. For the case of a classic bi-Maxwellian ($\beta = 0$), the expression simplifies to $A = \frac{p_{th_{\perp}}^2}{p_{th_{\parallel}}^2} - 1 = \frac{T_{\perp}}{T_{\parallel}} - 1$, which readily conveys the concept of anisotropy or directional dependence of the distribution. For a bi-Maxwellian, without the loss cone, if the perpendicular and parallel temperatures (thermal velocities) are equal, the anisotropy is identically zero. Thus, waves are unstable to the plasma if the electron temperature is higher in the direction perpendicular to the magnetic field than parallel to it. For this reason, the term “temperature anisotropy” is used since it provides simple physical intuition behind why the waves are unstable. In the general case of a subtracted bi-Maxwellian, the pitch angle anisotropy will always be higher than that of a classic bi-Maxwellian and one can have anisotropy just from the presence of the loss cone even if thermal temperatures are in equilibrium.

4 Results

We first use BTP model to explore a small number of particle trajectories as has been done in other works using forward time stepping methods (Inan, 1977; Albert, 2002; Tao et al., 2012) to illustrate some basic physical phenomena. The test particle trajectories will be compared to the linearized equations of motion to emphasize the need for a scattering model which includes both linear and nonlinear effects. Afterwards, the backward test particle model is used to investigate particle scattering and dynamics of the distribution function.

4.1 Test particle trajectories

The BTP code used in the context of a test particle simulation basically treats a few phase space points as test particles and traces them backwards to create the trajectories. Tracing the test particles backward is done by solving the exact same equations of motion as in the BTP approach, but instead of a lot of particles sampled to represent the distribution function, only a few test particles are evaluated to examine their motion in phase (velocity) space.

Figure 4 shows test particle trajectories for a monochromatic constant amplitude wave. The trajectories using the nonlinear expressions (panel b) are compared to those obtained when the equations of motion are linearized around the adiabatic motion (panel a) [Harid et al., 2014, Appendix A, Equations A6-A7]. As is shown in the left panel (Figure 4A), for an assumed dipole geomagnetic field, the phase trapped resonant particles do not appear in the linearized trajectories. All particles are uniformly distributed in gyrophase with the same value of v_{\perp} starting at the same initial position. The initial gyrophase angle when a particle goes into resonance with the wave determines whether the particle is phase trapped or not. As is shown in Figure 4B, untrapped particles are deflected as they come into resonance with the wave, while phase trapped stay in resonance with the wave longer before they are released from the trap. These phase trapped particles are seen to follow the resonance curve even when it departs significantly from the adiabatic motion followed by the untrapped particles.

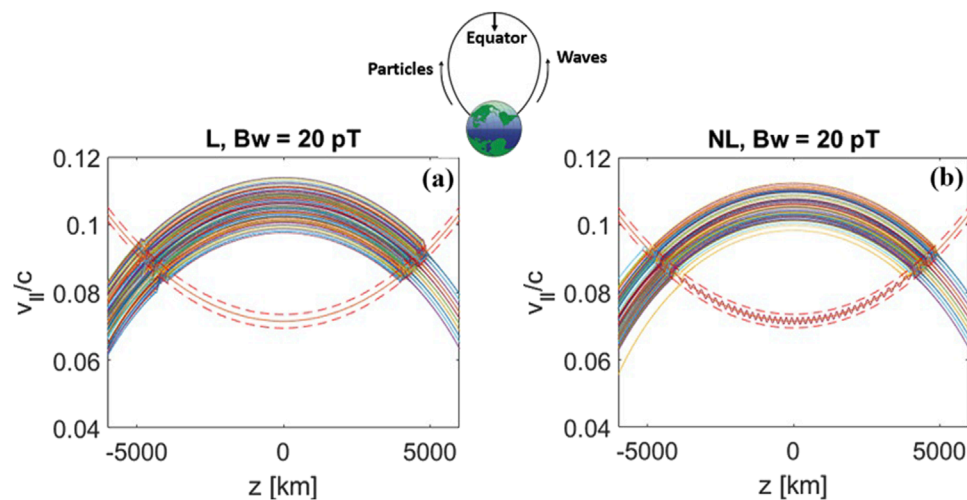


FIGURE 4

Linear L, panel (A) and nonlinear NL, panel (B) test particle trajectories for a monochromatic constant amplitude wave. In both cases, the majority of particles follow adiabatic motion along the rainbow shaped curve, with only slight perturbations when they intersect the orange resonance curve. In the nonlinear (NL) case (panel b), a few particle trajectories are visible along the orange cyclotron resonance curve. These particles are phase trapped and forced to stay in resonance with the wave.

Trapped particles deviate drastically from their adiabatic trajectories which in turn significantly modify the distribution function (Dowden et al., 1978; Omura and Summers, 2006; Chen et al., 2024a). For these reasons, phase trapping is believed to be a key component of nonlinear effects in wave-particle interaction.

The phase trapped particles are released when the geomagnetic gradient increases to a level where the trapping condition ($|S| < 1$) no longer holds. A higher wave amplitude can keep the particles trapped longer. The concept of “Trap-Release” has been demonstrated in recent self-consistent models as a particularly important mechanism in feedback of wave growth and frequency change (Tao et al., 2021; Harid et al., 2022).

For a wave amplitude lower than nonlinear threshold, for instance $B_w = 5 pT$, phase trapping will not happen, and thus the linearized equations give the same results as the test particle trajectories, which is summarized in Figure 5. Therefore, particles scatter similarly in the linear regime (Figure 5A) and nonlinear regime (Figure 5B) when the wave amplitude is small (below the nonlinear threshold).

4.2 Short pulse - detrapping

In the previous section, we showed the test particle trajectories for the constant wave amplitude and the wave filling the entire simulation domain along the geomagnetic field. These simulation results demonstrate important physical concepts behind wave-particle interactions, such as phase trapping once the wave amplitude is above the nonlinear trapping threshold. A more typical scenario inspired by ground based observations is when a wave of limited duration propagates through the interaction region (Inan et al., 1982; Hosseini et al., 2017). More specifically, such monochromatic pulses are not long enough in time (or space) to fill

out the entire simulation domain, which introduces unique effects at the front and back end of the pulse.

Figure 6B shows the test particle trajectories for an injected traveling 0.5-s pulse with wave amplitude of 60 pT and compares it to a “long” pulse (Figure 6A) that fills the whole simulation space as the results in Section 4.1. Large amplitude (up to 3–8 nT) of whistler mode waves are reported from *in situ* observations (Wilson III et al., 2011; Santolik et al., 2014). Such waves can be naturally occurring chorus waves, waves from lightning or waves from transmitters. As is shown in Figure 6B, once the wave front reaches the particles location, some of the particles get phase trapped and stay in resonance with the wave until the back end of the traveling wave leaves the particle location. Once the particles that have been phase trapped by the travelling wave are let go by the wave (detrapping), they keep traveling on adiabatic trajectories. If the detrapped particles hold their phase-bunched (coherence) characteristic for a few trapping periods after they exit the wave field, they are capable of radiating either a falling or rising emission (Roux and Pellat, 1978). To be more specific, the phase-bunched particles traveling on adiabatic trajectories are capable of creating coherent resonant currents that radiate Doppler shifted frequencies in a manner of an end fire antenna (Helliwell and Crystal, 1973; Nunn, 1974). It is worth noting that at this stage (after detrapping) the injected wave has left the particles, and the radiated frequencies are associated with “free running” triggered waves (Harid et al., 2022; Tao et al., 2021).

If the conversion to adiabatic motion takes place before (after) the equator toward a region of lower (higher) gyrofrequency, the radiated frequencies are frequency-time risers (fallers). This finding is consistent with change of fallers to risers in the experimental data when transmitted pulse duration is changed (Li et al., 2014). Specifically, Helliwell and Katsufakis (1974) showed that fallers are generated by short pulses up to 250 ms in duration and risers are generated by longer pulses 300–400 ms long. This simple yet elegant model was originally put forth by Roux and Pellat [1978]. The caveat

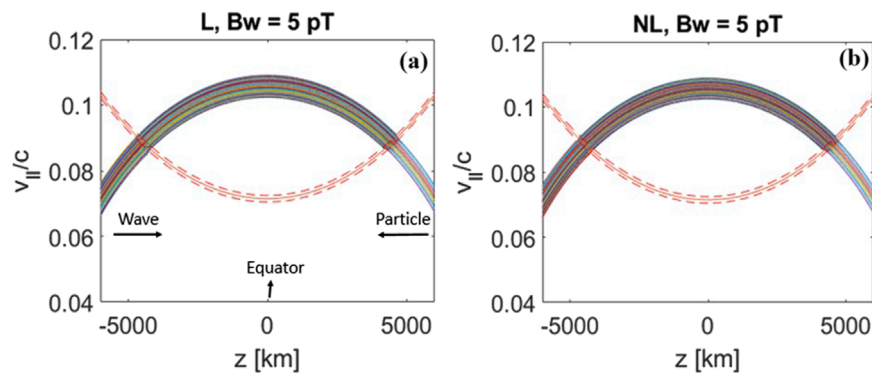


FIGURE 5 Test particle trajectories for a monochromatic constant lower (5 pT) amplitude wave. For this lower amplitude the (A) linear and (B) nonlinear models yield the same results.

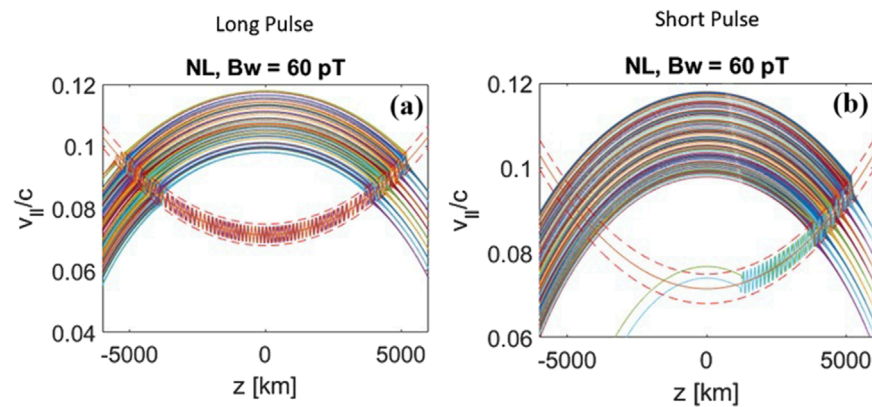


FIGURE 6 Test particle trajectories for an injected short (0.5 s) pulse with wave amplitude of 60 pT right panel (B) compared to a “long” pulse left panel (A) that fills the simulation space.

is that the detrapped electrons will quickly mix in gyrophase, so the distance over which coherent radiation takes place would have to be small. There are more complicated theories of risers versus fallers that are based on coherent radiation by phase trapped particles while being forced in resonance with the wave but on different sides of the equator (Nunn and Omura, 2012). In either case, the magnitude and position of wave amplitude spatial gradients along the field aligned propagation path is seen as a key parameter.

The above-described backward test particle (BTP) simulation demonstrates some important physical concepts of individual particle motion such as phase trapping, detrapping, and the possibility of end-fire antenna radiation. In this section, we use the BTP approach which solves the same equations of motion for sampled phase space grid points to represent the distribution function. This backward scheme thus investigates the dynamic of the phase space distribution function for a counter-streaming whistler mode pulse.

The shape of the phase space trap changes along the geomagnetic field line. The top panels (d-f) of Figure 7 shows the structure of the phase space trap at several position along the field line for a monochromatic constant amplitude whistler mode wave. As a

reminder, ζ represents gyrophase and the vertical axis is defined by a normalized deviation of $v_{||}$ from resonance, as Equation 20:

$$\zeta = \frac{k(v_{||} - v_r)}{\sqrt{2}\omega_{tr}} \tag{20}$$

where zero value on the vertical axis corresponds to the resonance velocity. The closed curves in phase-space correspond to the trapped trajectories that are separated by the separatrix from the open curves representing untrapped particles. The separatrix is shown on the contours as a red dashed line in the top panels of Figures 7D–F. Trapped particles that are forced to remain in resonance from their initial contact with the wave for a long period of time, moving toward the equator, drag the value of their distribution function to phase space locations that are upstream. Here, downstream is the direction of the wave propagation, the resonant particles travel in the opposite direction so they travel upstream, As shown in the test particle (see Figure 4), electrons that are trapped downstream of the wave will start at a higher value of $v_{||}$ and follow the resonance curve to lower values of $v_{||}$ around the magnetic equator. Since the initial velocity distribution (e.g., the subtracted bi-Maxwellian

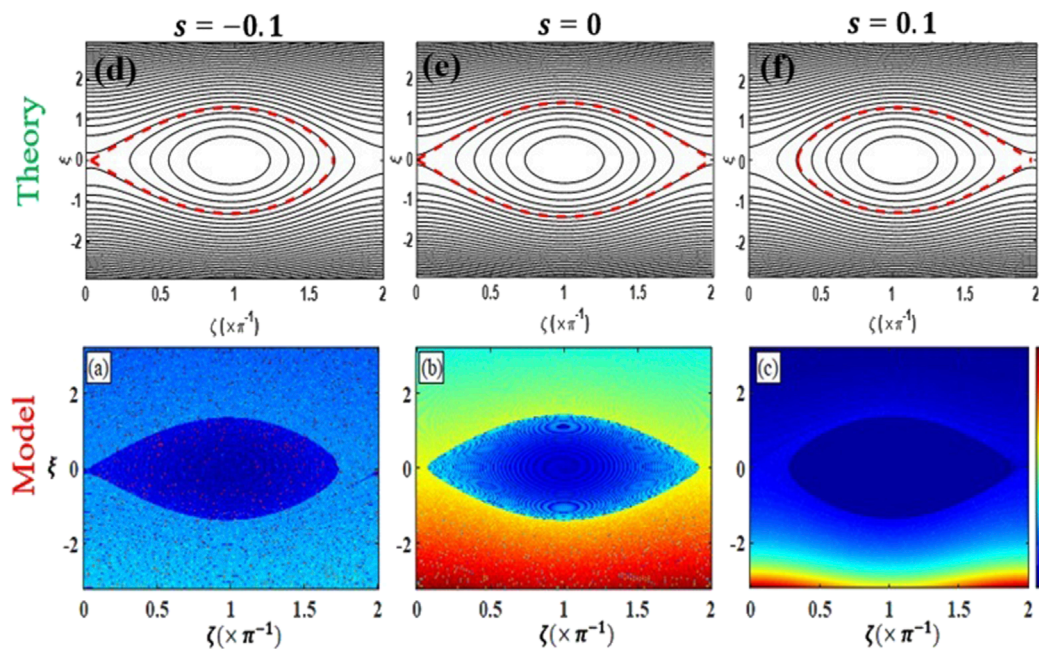


FIGURE 7 Formation of phase-space electron hole from test particle trajectories. (A) upstream location, (B) equator, and (C) downstream location relative to the wave propagation direction compared to theory (D–F).

distribution Figure 3, or any realistic distribution) has a lower value at higher particle velocities, the density inside the trap at the equator will be much lower than the surrounding regions of phase-space. This results in what is known as an “electron hole” in phase-space (Omura et al., 2008; Chen et al., 2024b; Ozaki et al., 2024).

By running test particle trajectories backwards in time, and using Liouville’s theorem, the distribution function can be reconstructed in high resolution. It is important to note that running the simulation backwards in time means that we can have arbitrary resolution of the perturbed distribution as this maps to known coordinates of the known initial distribution. In contrast, when simulations are run forward in time, it is not clear how finely the initial distribution must be sampled in phase space to capture all salient features of the disturbed distribution. For the case of a monochromatic and constant amplitude wave, the bottom panels of Figures 7A–C shows the electron hole for three different locations along the field line (upstream (a), equator (b), and downstream (c) of the wave). It is worth noting that the concept of $t = 0$ for a constant amplitude wave happens when the wave enters the wave-particle interaction region. As shown, the electron hole is well-defined and has an approximately constant density (i.e., phase-mixed) inside the phase-space trapping region while the region outside the trap will be close to the unperturbed velocity distribution.

One should note that for a short pulse (or higher pitch angles) the opposite can occur and an “electron hill” can be formed as well (Nunn and Omura, 2012; Hikishima and Omura, 2012). It is worth noting that the trapping mechanism transports one region of phase space to another, carrying with it the phase space density from one location and displacing the one that would be there

from adiabatic motion. Whether a hole or hill is formed depends on where the particles are initially trapped and the value of their resonance velocity when they are released as compared to the adiabatic background. Here the wave has sufficient amplitude that the leading edge of the wave pulse immediately phase traps electrons that are locally resonant. The initial location of trapping is a function of time, changing as the wave propagates downstream. The electrons will be de-trapped when they are no longer under the influence of the wave. Therefore, where the electrons exit the trap depends on the length of the pulse in time which is proportional to its length in physical space. The exit location also changes in time and can be before the particles reach the equator, at the equator or upstream of the equator on the other side. For a constant frequency considered here, a phase space hole is formed for particles trapped downstream of the equator and released on the downstream side of the equator or at the equator. A hill will be formed if particles are released upstream of the equator. Such electrons are trapped initially closer to the equator and released farther away so they are transported to a higher resonant velocity. In the above discussion we have assumed that the pitch angles are low enough so that they do not limit the interaction length with the wave. Higher pitch angles limit the interaction length, so they have the same effect as a shortened pulse length.

For a monochromatic constant wave amplitude higher than the trapping threshold, the electron hole exists when $-1 < S < 1$ and its shape changes along the geomagnetic field line. It is worth noting that for rising or falling frequency tone waves, the shape of the hole or hill could remain unchanged. For short pulses, since the wave only fills certain locations along the geomagnetic field line, the phase-space hole formation also depends on the presence of the traveling wave and its time span. That is, the phase-space hole/hill starts

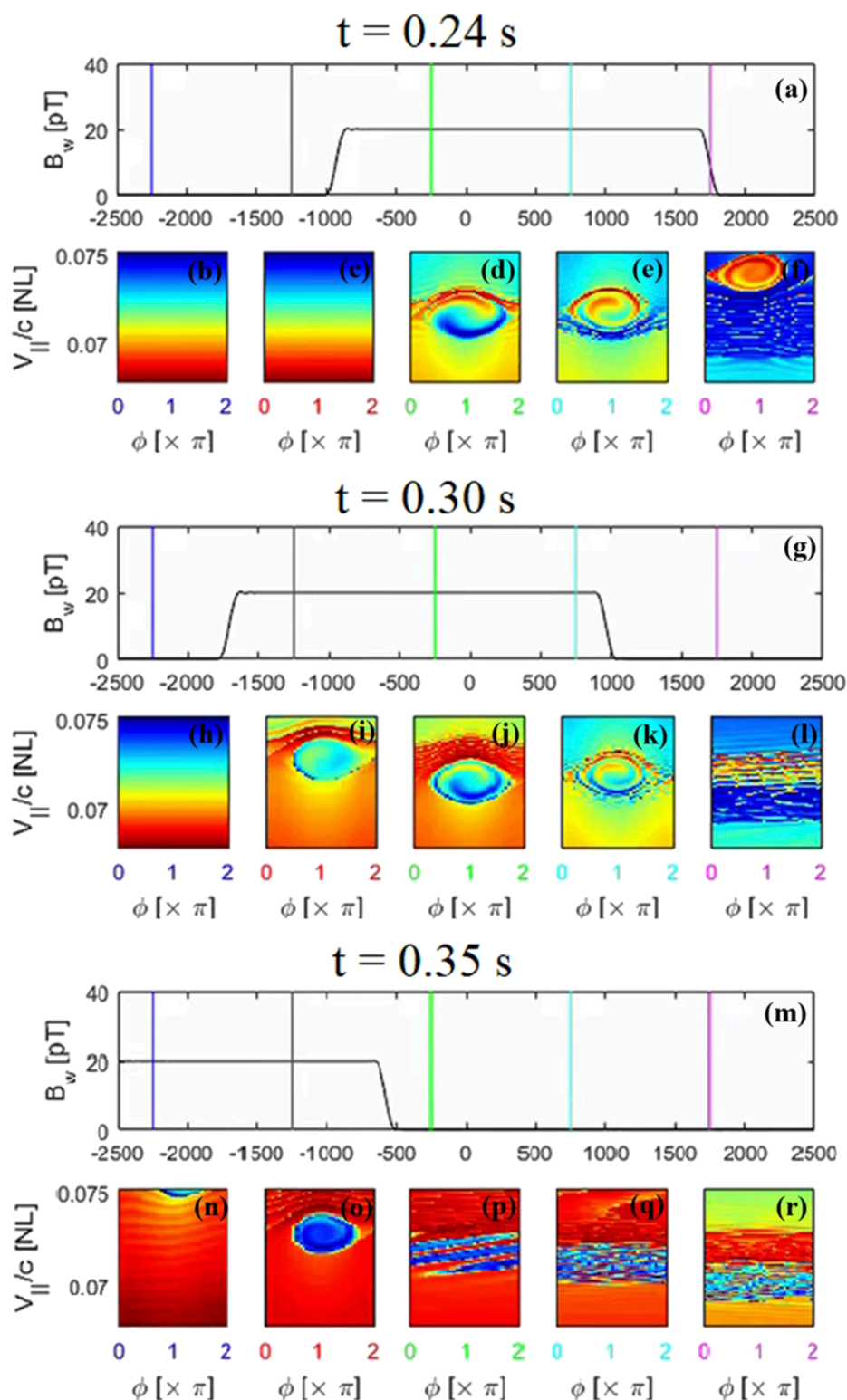


FIGURE 8 Phase space distribution for five different locations [$z = 1,750$ km (F, L, R), 750 km (E, K, Q), -250 km (D, J, P), $-1,250$ km (C, I, O), and $-2,250$ km (B, H, N)] along the field line at three specific times [$t = 0.24$ s (A), 0.30 s (G), and 0.35 s (M)].

forming once the traveling wave front reaches the counter-streaming particles and stays until the back end of the pulse leaves the particles' location. Once the wave is gone, the phase trapped particles are getting detrapped and keep moving on adiabatic trajectories.

Figure 8 shows the phase space distribution for five different locations along the field line ($z = 1,750$, 750 , -250 , $-1,250$, and $-2,250$ km) at three specific times ($t = 0.24$ s (Figure 8A), 0.30 s (Figure 8G), and 0.35 s (Figure 8M) after injection of a

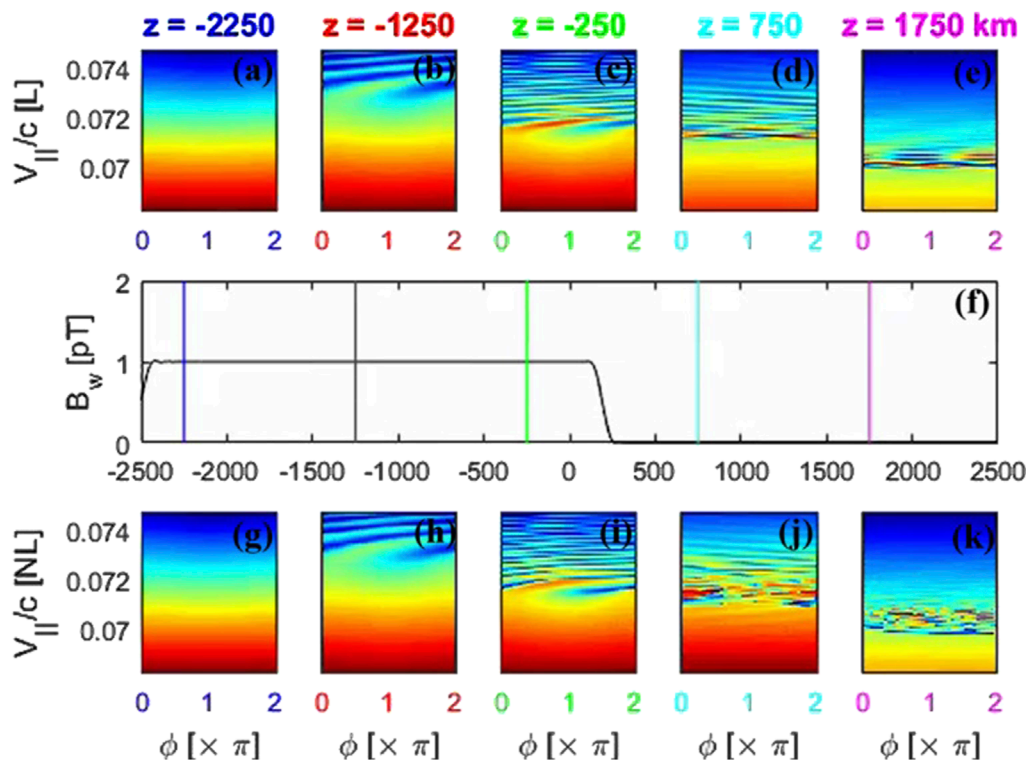


FIGURE 9 Linear scattered particle distribution (top a-e panels) for five different locations [$z = 1,750$ km (A), 750 km (B), -250 km (C), $-1,250$ km (D), and $-2,250$ km (E)] along the field line at (F) $t = 0.30$ s compared with the nonlinear scattering case [bottom (G-K) panels] for a monochromatic half a second pulse with $1pT$ wave amplitude.

monochromatic 0.5 s pulse. At $t = 0.24$ s (Figures 8B–F) the pulse mainly only fills out the upstream locations (first two locations in panel e and f) which creates an electron hill at the resonance velocity of each location. One can see that the electron hill at $z = 1750$ km (panel f) is formed at higher velocity range than the $z = 750$ km (panel e) location. It is worth noting that the color scale used in Figures 8–10 is the same as Figure 3.

At $t = 0.30$ s (Figures 8H–L) the pulse has left the $z = 1750$ km location (panel l) and the electron hill is washed out. However, the pulse is still passing over the three middle locations (panels i–k) and thus we see the formation of an electron hole (hill) at the upstream (downstream) locations corresponding to $z = -250, -1250$ km ($z = 750$ km). This is due to the fact that trapped particles are forced to stay in resonance with the wave and will drag the downstream value of the distribution function to locations that are upstream.

At $t = 0.35$ s (Figures 8N–R) the wave is only passing over the two furthest negative locations (panels n and o) and there is an electron hole at both locations, but the one located at $z = -2250$ km (panel n) is partially outside of the phase space simulation domain. In general, once the wave leaves each location, the created electron hill (hole) starts to wash away and shifts to lower (higher) velocities due to the adiabatic motion of the detrapped particles. For example, considering the phase space distribution at $z = -2250$ km for all three timeframes (panels b, h, and n), one can see that the electron hill created at $v_{||} = 0.074c$ washes away to a distribution enhancement strip around $v_{||} = 0.073c$. The velocity shift is associated with the

detrapped particles moving on adiabatic trajectories after being let go by the wave.

5 Comparison to linear theory

As mentioned before, phase trapping is a nonlinear process and therefore is not in the scope of linear scattering theory. The distribution function is calculated when particles are linearly scattered by the wave. The linearly scattered distribution can be reconstructed by running test particle trajectories backwards in time over linearized equations of motion and employing Liouville’s theorem. The goal was to be able to compare the distribution dynamic in the linear regime with the results when full equations of motion are considered in constructing the distribution function.

Figure 9 shows the Linear scattered particle distribution (top a-e panels) for five different locations ($z = 1750, 750, -250, -1,250,$ and $-2,250$ km) along the field line at $t = 0.30$ s along with the nonlinear scattering case (bottom g-k panels) for a monochromatic half a second pulse with $1pT$ wave amplitude. As is shown in Figures 9A–E, the linearized equations of motion give the same results as the nonlinear model (Figures 9G–K). This is expected when the wave amplitude shown in Figure 9F is below the phase trapping threshold. In general, since the wave amplitude can grow to values larger than the phase trapping threshold (Bell and Inan, 1981), the scattering model should solve the full equations of motion.

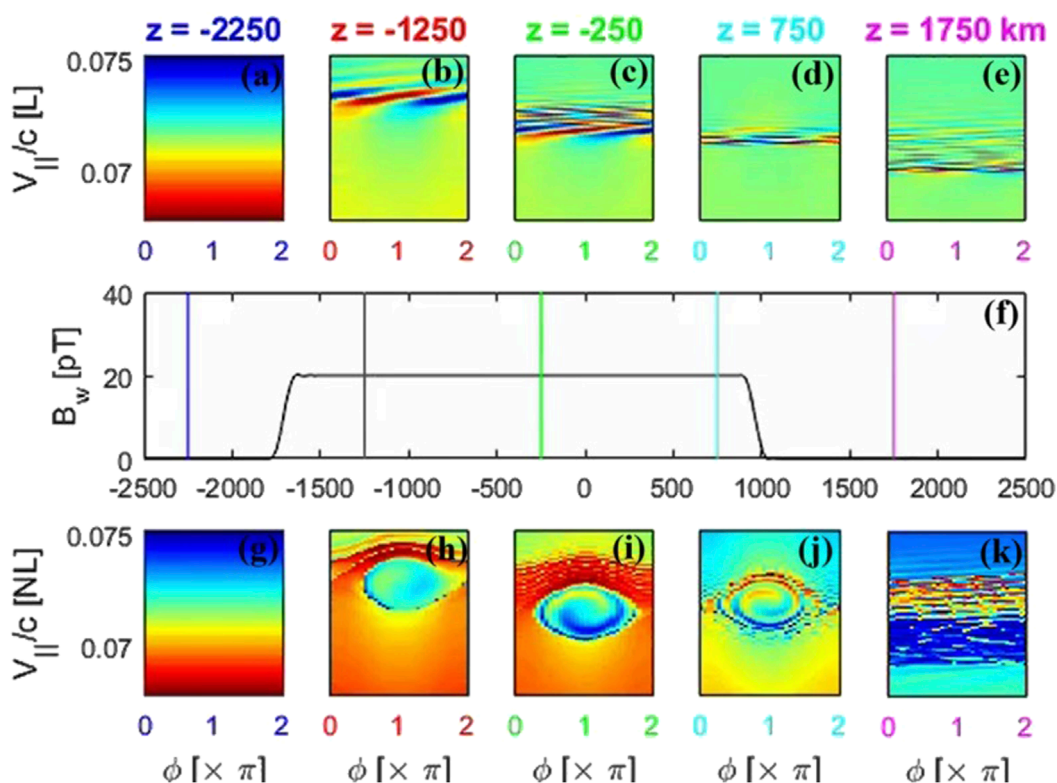


FIGURE 10 Linear scattered particle distribution (top a–e panels) for five different locations [$z = 1,750$ km (A), 750 km (B), -250 km (C), $-1,250$ km (D), and $-2,250$ km (E)] along the field line at (F) $t = 0.30$ s comparing with the nonlinear scattering case [bottom (G–K) panels] for a monochromatic half a second pulse with $1pT$ wave amplitude.

There is no formation of phase-space hole and both models show features that can be characterized as linear striations or ripples in phase-space.

Following the previous Figure setup, Figure 10 shows the distribution function for a $20pT$ wave amplitude while other simulation parameters remain unchanged. No electron hole or hill shows up in the linear case (panels a–e) since phase trapping cannot be considered within the scope of linear scattering theory (linearized equations of motion).

6 Conclusion

We developed a backward test particle numerical model that calculates scattering of the energetic electrons distribution by coherent whistler mode waves. This model requires specifying the wave fields *a priori* and is quite useful at evaluating the effect of waves on the particles in terms of scattering. This study provides important insights into the nonlinear dynamics of wave-particle interactions in Earth’s radiation belts, particularly through the lens of coherent whistler wave instability and whistler mode wave amplification. By utilizing a backward test particle model, we have demonstrated the formation of distinct phase space structures, such as electron phase space holes, in the nonlinear regime, which are not present under linear conditions. These findings underscore the limitations of quasi-linear diffusion theory in capturing the full scope of wave-induced

perturbations. The differences observed between the linear and nonlinear perturbations confirm the significant role of nonlinear phase trapping in driving the amplification of whistler mode waves. Although, the presented model is not able to reproduce the effect of the particles on the wave’s amplitude and phase, the formation of nonlinear structures in phase-space can be obtained and analyzed and the expected radiation currents from the perturbed distribution can be evaluated. These results contribute to a more comprehensive understanding of radiation belt dynamics and the complex processes involved in particle acceleration and scattering, with implications for future studies in space weather modeling and the prediction of radiation belt behavior.

Data availability statement

The raw data supporting the conclusions of this article will be made available by the authors, without undue reservation.

Author contributions

PH: Formal Analysis, Visualization, Writing–original draft, Writing–review and editing. VH: Conceptualization, Methodology,

Supervision, Writing–review and editing. MG: Funding acquisition, Investigation, Project administration, Resources, Supervision, Writing–review and editing. WT: Funding acquisition, Resources, Writing–review and editing, Supervision.

Funding

The author(s) declare that financial support was received for the research, authorship, and/or publication of this article. The authors acknowledge support from NSF Award AGS 2312282 to University of Colorado Denver and NASA grants 80NSSC21K1312 and 80NSSC21K2008 to West Virginia University.

References

- Abel, B., and Thorne, R. M. (1998). Electron scattering loss in Earth's inner magnetosphere: 1. Dominant physical processes. *J. Geophys. Res.* 103, 2385–2396. doi:10.1029/97JA02919
- Albert, J. M. (1999). Analysis of quasi-linear diffusion coefficients. *J. Geophys. Res.* 104 (A2), 2429–2441. doi:10.1029/1998JA900113
- Albert, J. M. (2002). Nonlinear interaction of outer zone electrons with VLF waves. *Geophys. Res. Lett.* 29 (8), 116–1. doi:10.1029/2001gl013941
- Albert, J. M., Tao, X., and Bortnik, J. (2012). “Aspects of nonlinear wave-particle interactions,” in *Dynamics of the Earth's radiation belts and inner magnetosphere*. *Geophys. Monogr. Ser.* Editor D. Summers (Washington, D. C.: AGU), 199, 255–264. doi:10.1029/2012GM001324
- Bell, T. F. (1984). The nonlinear gyroresonance interaction between energetic electrons and coherent VLF waves propagating at an arbitrary angle with respect to the Earth's magnetic field. *J. Geophys. Res.* 89 (A2), 905–918. doi:10.1029/JA089iA02p00905
- Bell, T. F., and Buneman, O. (1964). Plasma instability in the whistler mode caused by a gyrating electron stream. *Phys. Rev.* 133, A1300–A1302. doi:10.1103/PhysRev.133.A1300
- Bell, T. F., and Inan, U. S. (1981). Transient nonlinear pitch angle scattering of energetic electrons by coherent VLF wave packets in the magnetosphere. *J. Geophys. Res. Space Phys.* 86 (A11), 9047–9063. doi:10.1029/ja086ia11p09047
- Bortnik, J., Thorne, R. M., and Inan, U. S. (2008). Nonlinear interaction of energetic electrons with large amplitude chorus. *Geophys. Res. Lett.* 35, L21102. doi:10.1029/2008GL035500
- Carpenter, D. L., and Anderson, R. R. (1992). An ISEE/whistler model of equatorial electron density in the magnetosphere. *J. Geophys. Res.* 97, 1097–1108. doi:10.1029/91JA01548
- Chen, H., Wang, X., Chen, L., Zhang, X. J., Omura, Y., Chen, R., et al. (2024a). Nonlinear electron trapping through cyclotron resonance in the formation of chorus subpackets. *Geophys. Res. Lett.* 51 (11), e2024GL109481. doi:10.1029/2024gl109481
- Chen, H., Wang, X., Zhao, H., Lin, Y., Chen, L., Omura, Y., et al. (2024b). Electron dynamics associated with advection and diffusion in self-consistent wave-particle interactions with oblique chorus waves. *Geophys. Res. Lett.* 51 (14), e2024GL110362. doi:10.1029/2024gl110362
- Dowden, R. L., McKay, A. D., Amon, L. E. S., Koons, H. C., and Dazey, M. H. (1978). Linear and nonlinear amplification in the magnetosphere during a 6.6-kHz transmission. *J. Geophys. Res. Space Phys.* 83 (A1), 169–181. doi:10.1029/ja083ia01p00169
- Dysthe, K. B. (1971). Some studies of triggered whistler emissions. *J. Geophys. Res.* 76 (28), 6915–6931. doi:10.1029/JA076i028p06915
- Fu, S., Ni, B., Zhou, R., Cao, X., and Gu, X. (2019). Combined scattering of radiation belt electrons caused by Landau and bounce resonant interactions with magnetosonic waves. *Geophys. Res. Lett.* 46 (17–18), 10313–10321. doi:10.1029/2019gl084438
- Gendrin, R. (1981). General relationships between wave amplification and particle diffusion in a magnetoplasma. *Rev. Geophys.* 19 (1), 171–184. doi:10.1029/RG019i001p00171
- Gibby, A. R., Inan, U. S., and Bell, T. F. (2008). Saturation effects in the VLF-triggered emission process. *J. Geophys. Res.* 113, A11215. doi:10.1029/2008JA013233
- Golkowski, M., Harid, V., and Hosseini, P. (2019). Review of controlled excitation of non-linear wave-particle interactions in the magnetosphere. *Front. Astronomy Space Sci.* 6, 2. doi:10.3389/fspas.2019.00002
- Harid, V., Golkowski, M., Bell, T., and Inan, U. S. (2014). Theoretical and numerical analysis of radiation belt electron precipitation by coherent whistler mode waves. *J. Geophys. Res. Space Phys.* 119 (6), 4370–4388. doi:10.1002/2014ja019809
- Harid, V. (2015). Coherent interactions between whistler mode waves and energetic electrons in the Earth's radiation belts: Stanford University
- Harid, V., Golkowski, M., Hosseini, P., and Kim, H. (2022). Backward-propagating source as a component of rising tone whistler-mode chorus generation. *Front. Astronomy Space Sci.* 9, 981949. doi:10.3389/fspas.2022.981949
- Helliwell, R. A. (1965). VLF wave stimulation experiments in the magnetosphere from Siple Station, Antarctica. *Rev. Geophys.* 26 (3), 551–578. doi:10.1029/RG026i003p00551
- Helliwell, R. A., and Crystal, T. L. (1973). A feedback model of cyclotron interaction between whistler-mode waves and energetic electrons in the magnetosphere. *J. Geophys. Res.* 78 (31), 7357–7371. doi:10.1029/ja078i031p07357
- Helliwell, R. A., and Katsufakis, J. P. (1974). VLF wave injection into the magnetosphere from Siple Station, Antarctica. *J. Geophys. Res.* 79 (16), 2511–2518. doi:10.1029/ja079i016p02511
- Hikishima, M., and Omura, Y. (2012). Particle simulations of whistler-mode rising-tone emissions triggered by waves with different amplitudes. *J. Geophys. Res. Space Phys.* 117 (A4). doi:10.1029/2011ja017428
- Hikishima, M., Omura, Y., and Summers, D. (2010). Self-consistent particle simulation of whistler mode triggered emissions. *J. Geophys. Res.* 115, A12246. doi:10.1029/2010JA015860
- Hosseini, P., Golkowski, M., and Turner, D. L. (2017). Unique concurrent observations of whistler mode hiss, chorus, and triggered emissions. *J. Geophys. Res. Space Phys.* 122, 6271–6282. doi:10.1002/2017ja024072
- Hu, G., and Krommes, J. A. (1994). Generalized weighting scheme for δf particle-simulation method. *Phys. plasmas* 1 (4), 863–874. doi:10.1063/1.870745
- Inan, U. S. (1977). *Non-linear gyroresonant interactions of energetic particles and coherent VLF waves in the magnetosphere* Doctoral dissertation. Stanford University.
- Inan, U. S., Bell, T. F., and Chang, H. C. (1982). Particle precipitation induced by short-duration VLF waves in the magnetosphere. *J. Geophys. Res.* 87, 6243–6264. doi:10.1029/JA087iA08p06243
- Inan, U. S., Bell, T. F., and Helliwell, R. A. (1978). Nonlinear pitch angle scattering of energetic electrons by coherent VLF waves in the magnetosphere. *J. Geophys. Res.* 83 (A7), 3235–3253. doi:10.1029/JA083iA07p03235
- Katoh, Y., and Omura, Y. (2007). Computer simulation of chorus wave generation in the Earth's inner magnetosphere. *Geophys. Res. Lett.* 34, L03102. doi:10.1029/2006GL028594
- Kennel, C. F., and Petschek, H. E. (1966). Limit on stably trapped particle fluxes. *J. Geophys. Res.* 71, 1–28. doi:10.1029/jz071i001p00001
- Li, J. D., Spasojevic, M., Harid, V., Cohen, M. B., Golkowski, M., and Inan, U. (2014). Analysis of magnetospheric ELF/VLF wave amplification from the Siple Transmitter experiment. *J. Geophys. Res. Space Phys.* 119 (3), 1837–1850. doi:10.1002/2013ja019513
- Lyons, L. R., Thorne, R. M., and Kennel, C. F. (1972). Pitch-angle diffusion of radiation belt electrons within the plasmasphere. *J. Geophys. Res.* 77 (19), 3455–3474. doi:10.1029/JA077i019p03455
- Maldonado, A. A., Chen, L., Claudepierre, S. G., Bortnik, J., Thorne, R. M., and Spence, H. (2016). Electron butterfly distribution modulation by magnetosonic waves. *Geophys. Res. Lett.* 43 (7), 3051–3059. doi:10.1002/2016gl068161

Conflict of interest

The authors declare that the research was conducted in the absence of any commercial or financial relationships that could be construed as a potential conflict of interest.

Publisher's note

All claims expressed in this article are solely those of the authors and do not necessarily represent those of their affiliated organizations, or those of the publisher, the editors and the reviewers. Any product that may be evaluated in this article, or claim that may be made by its manufacturer, is not guaranteed or endorsed by the publisher.

- Matsumoto, H., and Omura, Y. (1981). Cluster and channel effect phase bunchings by whistler waves in the nonuniform geomagnetic field. *J. Geophys. Res.* 86 (A2), 779–791. doi:10.1029/JA086iA02p00779
- Nunn, D. (1974). A self-consistent theory of triggered VLF emissions. *Planet. Space Sci.* 22, 349–378. doi:10.1016/0032-0633(74)90070-1
- Nunn, D., and Omura, Y. (2012). A computational and theoretical analysis of falling frequency VLF emissions. *J. Geophys. Res. Space Phys.* 117 (A8). doi:10.1029/2012ja017557
- Nunn, D., and Omura, Y. (2015). A computational and theoretical investigation of nonlinear wave-particle interactions in oblique whistlers. *J. Geophys. Res. Space Phys.* 120 (4), 2890–2911. doi:10.1002/2014ja020898
- Omura, Y., Katoh, Y., and Summers, D. (2008). Theory and simulation of the generation of whistler-mode chorus. *J. Geophys. Res.* 113, A04223. doi:10.1029/2007JA012622
- Omura, Y., Matsumoto, H., Nunn, D., and Rycroft, M. J. (1991). A review of observational, theoretical and numerical studies of VLF triggered emissions. *J. Atmos. Terr. Phys.* 53, 351–368. doi:10.1016/0021-9169(91)90031-2
- Omura, Y., and Nunn, D. (2011). Triggering process of whistler mode chorus emissions in the magnetosphere. *J. Geophys. Res.* 116, A05205. doi:10.1029/2010JA016280
- Omura, Y., and Summers, D. (2006). Dynamics of high-energy electrons interacting with whistler mode chorus emissions in the magnetosphere. *J. Geophys. Res. Space Phys.* 111 (A9). doi:10.1029/2006ja011600
- Ozaki, M., Mizote, K., Kondo, T., Yagitani, S., Hikishima, M., and Omura, Y. (2024). Suppression of nonlinear chorus wave growth by active control of gyroresonant interactions with electron hole deformation. *Geophys. Res. Lett.* 51, e2024GL112218. doi:10.1029/2024GL112218
- Roux, A., and Pellat, R. (1978). A theory of triggered emissions. *J. Geophys. Res.* 83 (A4), 1433–1441. doi:10.1029/JA083iA04p01433
- Santolík, O., Kletzing, C. A., Kurth, W. S., Hospodarsky, G. B., and Bounds, S. R. (2014). Fine structure of large-amplitude chorus wave packets. *Geophys. Res. Lett.* 41 (2), 293–299. doi:10.1002/2013gl058889
- Summers, D. (2005). Quasi-linear diffusion coefficients for field-aligned electromagnetic waves with applications to the magnetosphere. *J. Geophys. Res.* 110, A08213. doi:10.1029/2005JA011159
- Tao, X., Bortnik, J., Albert, J. M., and Thorne, R. M. (2012). Comparison of bounce-averaged quasi-linear diffusion coefficients for parallel propagating whistler mode waves with test particle simulations. *J. Geophys. Res. Space Phys.* 117 (A10). doi:10.1029/2012ja017931
- Tao, X., Zonca, F., and Chen, L. (2021). A “trap-release-amplify” model of chorus waves. *J. Geophys. Res. Space Phys.* 126 (9), e2021JA029585. doi:10.1029/2021ja029585
- Wang, X., Chen, H., Omura, Y., Hsieh, Y. K., Chen, L., Lin, Y., et al. (2024). Resonant electron signatures in the formation of chorus wave subpackets. *Geophys. Res. Lett.* 51 (8), e2023GL108000. doi:10.1029/2023gl108000
- Wilson III, L. B., Cattell, C. A., Kellogg, P. J., Wygant, J. R., Goetz, K., Breneman, A., et al. (2011). The properties of large amplitude whistler mode waves in the magnetosphere: propagation and relationship with geomagnetic activity. *Geophys. Res. Lett.* 38 (17). doi:10.1029/2011gl048671